Broadband Bias-Magnet-Free On-Chip Optical Isolators With Integrated Thin Film Polarizers

Dolendra Karki, Vincent Stenger, Andrea Pollick, and Miguel Levy

***Abstract*—Most on-chip optical isolators utilize nonreciprocal magneto-optic (MO) garnet-materials that require an external bias magnetic field to operate. The magnetic field is applied through incorporation of either a permanent magnet or an active electromagnet. Permanent magnets add significantly to device bulk and electromagnets increase fabrication complexity and power consumption. Hence, it is highly desirable to reduce or eliminate the magnetizing component in these devices. Here, we experimentally demonstrate a first of its kind bias-magnet-free (BMF) on-chip waveguide optical isolator with integrated Polarcor UltraThin polarizers. The BMF isolator device obviates the need for magnetizing components while possessing superior performance, relative to other on-chip isolators, with $\geq$25 dB of isolation ratio (IR), and $\leq$3.5 dB of insertion loss (IL) across the entire infrared optical C-band.**

***Index Terms*—Integrated waveguide devices, magneto-optic devices, nonreciprocal optics, optical isolators, optical waveguides.**

I. Introduction

IN PHOTONIC integrated circuits (PICs), optical isolators are essential components to block reflected feedback and protect active components such as semiconductor lasers and optical amplifiers for smooth operation. Most of the promising results in passive on-chip optical isolator development have been achieved by the use of magneto-optic materials, mainly bismuth- or cerium-substituted yttrium iron garnets (Bi:YIG or Ce:YIG). Significant progress has been made to integrate these materials onto silicon PIC platforms by sputtering or pulsed laser deposition [1]–[5] and by direct wafer bonding [6]–[8].

The polycrystalline nature of garnets grown on lattice and thermal mismatched substrate platforms via sputtering or pulsed-laser-deposition techniques offer lower magneto-optic efficiency and suffer from higher optical loss compared to those grown on lattice matched substrates via liquid-phase-epitaxy [9], [10]. Deposited garnets require additional design and material integration to minimize losses and for enhancement of the MO effect [10]. Hybrid bonding makes it possible to integrate high-quality single crystal garnets grown on lattice matched substrates as the upper cladding of the Si waveguide. However, this upper cladding geometry tends to limit hybrid bond technology to transverse magnetic (TM) mode devices. Most active components in photonic integrated circuits (PICs) operate on transverse electric (TE) mode of polarization and would require TE-TM mode converters to access the top MO film cladding on Si [11]–[13].

There have also been efforts to realize TE mode operating waveguide isolators by lateral deposition of cladding MO material using complex monolithic fabrication processes. In this lateral asymmetry geometry, the magnetization of the MO film is along the hard axis and requires magnetic fields in the $\geq 1KOe$ range to operate [14], [15]. Moreover, the lateral deposition method yields lower quality MO films resulting in larger device footprints relative to surface growth geometries. Nonreciprocal-phase-shift (NRPS) based devices incorporate either optical interference [7], [16]–[18], resonance effects [10], [14], [19], [20] or rely on implementations of topological edge states [21]. Mach Zehnder Interferometer (MZI)-based isolators result in relatively large device footprints whereas resonators, while featuring smaller device footprints, are not suitable for broadband applications. Topological edge states based isolators are considered robust against fabrication tolerances but require high NRPS performance to achieve small isolator device footprints [21].

Faraday rotation (FR) based optical isolators make use of MO material as the core of the waveguide structure and work for any polarization mode as long as it is linearly polarized. FR devices operate on the basis of conversion between TE and TM polarization modes. Commercially available optical isolators use the FR effect to offer large operating bandwidths along with high isolation ratios and low insertion losses [22]. The primary challenge in the FR approach for on-chip integrated optics is the suppression of polarization mode birefringence induced in asymmetric waveguide geometries. Alternating MO and non-MO materials along the optical path can mitigate this challenge through Quasi Phase matching (QPM) techniques [23], [24]. In today's 300 mm Si wafer technology, where device dimensions can be controlled to within a few nm, it is possible to directly fabricate waveguide geometries that are symmetric within required device tolerances [25].

An important feature that has not received as much attention has been downsizing the magnetizing element in most isolator prototypes [26]. Permanent magnets or electro-magnets are used to saturate the magnetization in the magneto-optical films for

Manuscript received July 31, 2019; revised October 3, 2019; accepted October 20, 2019. Date of publication October 24, 2019; date of current version February 12, 2020. This work was supported by the Air Force Research Laboratory under Contract FA8650-17-C-5072. *(Corresponding author: Miguel Levy.)*

D. Karki and M. Levy are with the Physics Department, Michigan Technological University, Houghton, MI 49931 USA (e-mail: dkarki@mtu.edu; mlevy@mtu.edu).

V. Stenger and A. Pollick are with SRICO, Inc., Columbus, OH 43235 USA (e-mail: vestenger@srico.com; apollick@srico.com).

Color versions of one or more of the figures in this article are available online at http://ieeexplore.ieee.org.

Digital Object Identifier 10.1109/JLT.2019.2949377

the nonreciprocal operation of the devices. These elements contribute considerable bulk to the optical isolator. Two main passive and active element approaches have been reported in the literature to address this bulk problem: (1) integration of the permanent magnet as a passive film element formed in the waveguide structure [26], and (2) integration of an electromagnet in the form of conducting wire of different shapes, depending on the device structure. In the case of the electro-magnet, tens of milli-Amps of current are injected to produce less than 100 Oe of bias magnetic field at the cost of raising the temperature and power consumption of the device [17], [27]. The heating of the wire on top of the MO material degrades the MO performance, which in turn requires the device to be longer. By operating the device below saturation magnetization, the current through the electromagnet can be regulated, via the linear MO effect, to compensate for temperature effects. However, currents on the order of Amps would be needed to produce the $\geq 1KOe$ fields needed for magnetization along the hard axis for TE mode operation. The associated heating is difficult to contain and is not desirable for integration with other potentially temperature sensitive components on a common PIC.

In this letter we report an alternative technology to address minimization of the bulk produced by the magnetizing element. In our case, we eliminate it altogether, while retaining full magneto-optic functionality. This bias-magnet-free (BMF) device is realized through the incorporation of latching iron garnet FR material, grown by liquid-phase-epitaxy (LPE), into an isolator device structure. Based on the FR effect, the device produces broadband functionality making it appealing for broadband applications. The key to BMF operation resides in the composition of the garnet, achieved through the incorporation of gallium and europium in order to reduce the saturation magnetization of the garnet without creating a compensation point [28], [29]. The nominal composition of the garnet is $Bi_x(Eu_zHo_{1-z})_{3-x}Fe_{5-y}Ga_yO_{12}$ per formula unit with $x \geq 1.2$, $0 \leq z \leq 0.45$, $0 \leq y \leq 5$ per formula unit such that the saturation magnetization ($4\pi M_s$) is between 10 to 60 Gauss.

Bismuth-substituted rare-earth iron garnets grown by liquid phase epitaxy along the $<111>$ direction possess a strong uniaxial growth-induced magnetic anisotropy. This type of anisotropy favors magnetization in the film parallel and anti-parallel to the growth direction. Competition between the demagnetizing energy and domain wall energy leads to the formation of magnetic domains, thus minimizing the free energy of the system. The application of an external magnetic field large enough to overcome the domain wall energy leads to the formation of a single domain saturated perpendicular to the plane of the film. However, lowering the magnetic moment of the film can also suppress domain formation by making the creation of domain walls too costly energetically. The demagnetizing energy can be reduced by diamagnetic doping of the iron sites, such as by gallium substitution, leading to a reduction in magnetic moment. Doping with holmium and europium also reduce the saturation magnetization and lower its temperature dependence. This means that the external magnetic field can be reduced below its saturation value without inducing domain formation, up to a certain point. For sufficiently small magnetization in the iron garnet, the magnitude of the sub-saturation external magnetic field required to prevent the formation of demagnetizing domains becomes negative, and eventually exceeds the negative saturation field of the material. This happens at saturation magnetization ($4\pi M_s$) below 100 G in these systems. At this point the material can only be made to switch between two single domain states with magnetizations pointing in opposite directions. This is called nucleation-induced-coercivity or latching. A very important feature of this process is that the switching field needed to flip the magnetization is approximately inversely proportional to the magnetization itself. This means that the coercive field can become quite large upon reducing the magnetization of the material. Further discussion of this phenomenon and its temperature dependence may be found in [28] and [29].

Previous work on this material has shown the preservation of magnetization and 45° Faraday rotation with $<$0.1 dB insertion loss in films down to 11 μm thickness fabricated by mechanical polishing [30]. Here we report on the implementation and performance of a fully functional waveguide isolator with integrated polarizers in latching MO material.

II. Methodology

A. Sample Processing

Latching bismuth iron garnet (BiIG) samples were acquired from II-VI, Inc. in the form of 10 mm $\times$ 10 mm $\times$ 480 μm plates, magnetized perpendicular to the plate surface. The plates were anti-reflection (AR) coated, front and back, and delivered approximately 45° Faraday rotation in the telecom C-Band wavelength range while propagating 480 μm along the normal direction to the sample plate surface.

Two 30 μm-thick Polarcor UltraThin glass polarizer films (Corning Inc.), polarization axes aligned at a 45° offset to each other, were bonded on opposite faces of the latching iron garnet samples using benzocyclobutene (BCB). BCB represented a robust and foundry-compatible process that could reliably withstand lapping and polishing processes without detaching the polarizers. One of the polarizers was bonded with its axis aligned to the desired input polarization while the second polarizer axis was aligned at 45° with respect to the first. Strips of material, 0.5 mm thick $\times$ 10 mm wide $\times$ 480 μm length, were diced from the assembly, with the magnetization direction along the 480 μm side. These strips were then thinned down and polished, via lapping, to produce thin slab waveguides, 12 μm thin $\times$ 10 mm $\times$ 480 μm in size. The 12 μm thin films were bonded with wax to a handle glass plate. Fig. 1 shows a top view of a polished film with polarizers attached.

B. Ridge Waveguides Fabrication

Ridge waveguides 12 to 15 μm wide with 3 to 8 μm ridge depths were patterned by focused ion beam (FIB) milling in 12 μm thin iron garnet films with and without bonded polarizers. Scanning electron micrograph (SEM) images of the ridge waveguide structures are shown in Fig. 2. Fig. 2(a) shows a ridge waveguide structure 12 μm in width and 3 μm ridge depth,

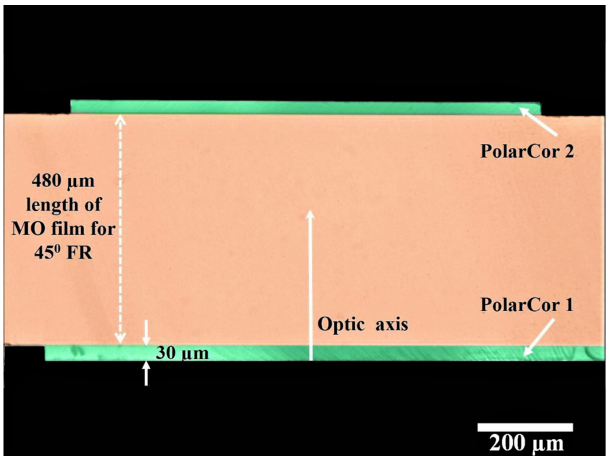

Fig. 1. Micrograph of top view of thin film slab waveguide isolator assembly with Polarcor polarizers attached to the front and back facets.

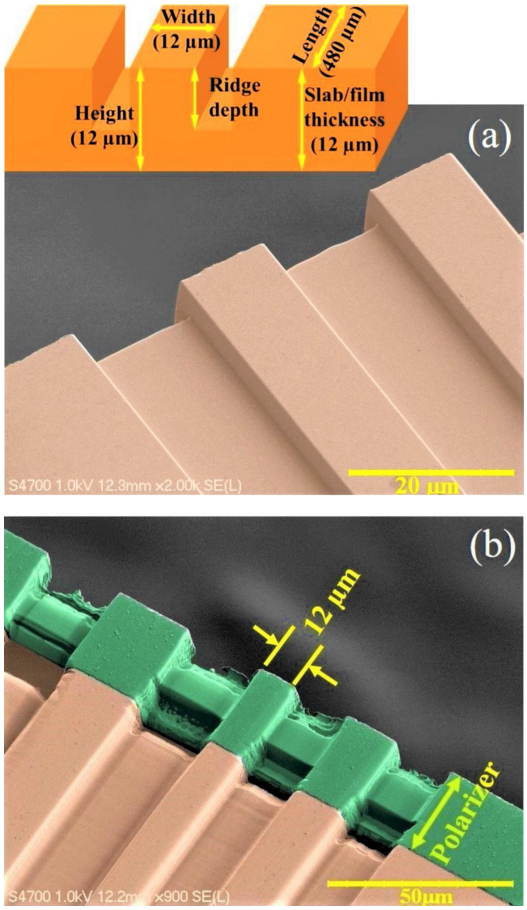

Fig. 2. Scanning-electron-microscopy image of an end facet of fabricated ridge waveguide (a) Faraday rotator and (b) isolator.

without attached polarizers. Fig. 2(b) shows the topography of a similar ridge waveguide device with Polarcor polarizers attached to the facets. As can be seen in Fig. 2(b), the ridges included polarizer film sections. Variations in the FIB removal rate caused a step in the milling depth at the polarizer/iron garnet interface.

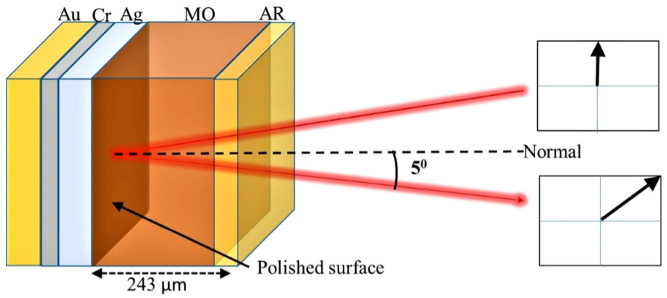

Fig. 3. Schematic of fabricated Faraday rotator mirror incorporating a metallic mirror coating on the back facet and anti-reflection coating (AR) on the front facet.

The erosion at the end facets in the milled region also made the trench length shorter than the waveguide core length near the outward ends.

C. Single-Sided Faraday Rotation Mirror

Experiments were conducted on Faraday rotator mirrors as a step towards reducing isolator device length and for implementing single-ended devices in which both input and output guides are along a single facet. Mirror-coating on one facet was used to make the light execute a double pass, forward and backward. This produced 45° of FR while reducing the thickness of the film in half (243 μm).

Sample pieces were thinned down to about 243 μm by lapping. The sample was thus left with only one AR coated surface, the AR coating having been removed during polishing from the other side. As for the mirror coatings, silver and gold metallic coatings yield high reflectance in the near-IR range. The reflectance of Au and Ag coatings were studied by directly depositing a 200 nm thin layer on a bare-glass substrate. The silver mirror produced a reflectance of 96% to 98% whereas that of the gold mirror was within 93% to 94% in the wavelength range 1480 nm to 1580 nm. Coatings of gold on 5 nm of Cr produced a reflectance below 90%. The polished surface of the sample was coated with 200 nm of Ag (e-beam evaporation) followed by 10 nm of Cr and 200 nm of Au (RF sputtering) as illustrated schematically in Fig. 3. The Cr-Au coating was to prevent the silver from tarnishing, which would degrade its reflectivity.

D. Optical Characterization

The optical test set-ups for slab and ridge waveguide structures and for Faraday rotators are shown schematically in Fig. 4(a) and Fig. 4(b), respectively. The set-ups consisted of a fiber pig-tailed tunable IR laser source, polarization controller, a lensed fiber coupling linearly polarized light into the optical isolator structure, a Glan-Thomson polarizer to analyze the angular-dependence of the output polarization, and an optical power meter. The output profiles from slab and ridge waveguides were observed on a display screen connected to the IR camera. Fig. 5 shows typical output profiles observed for the slab and ridge waveguide structures under study.

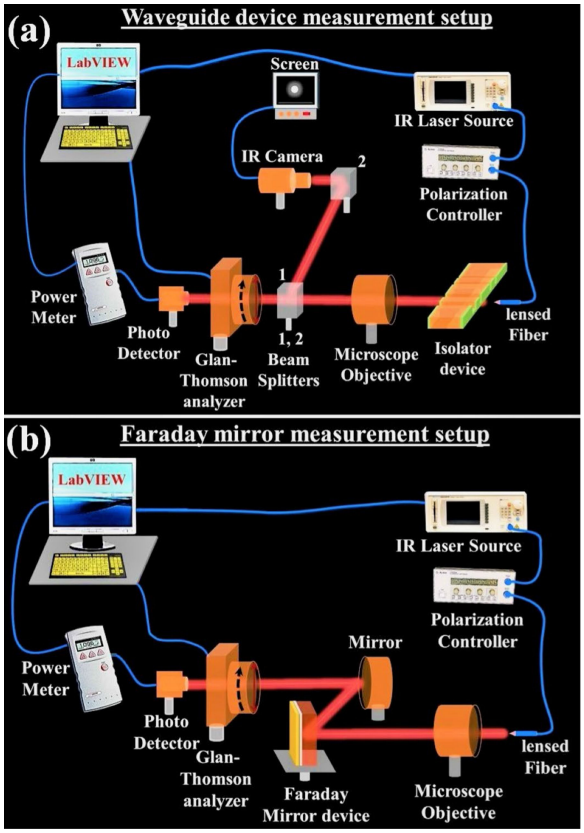

Fig. 4. Optical measurement setups (a) for slab and ridge waveguide structures and (b) for Faraday mirror.

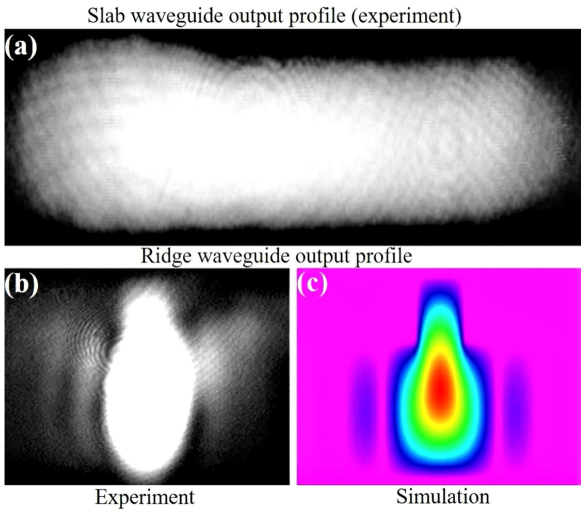

Fig. 5. IR camera images of output profiles observed in (a) slab waveguides, (b) ridge-waveguides. (c) Simulated fundamental mode output profile obtained by beam propagation method for a ridge waveguide of the same dimensions.

Optical isolation and insertion loss were measured between 1520 nm and 1580 nm. Optical isolation was defined as transmitted power in the backward propagation direction divided by forward power through the device. Insertion loss was defined as the ratio of transmitted power in the forward direction to

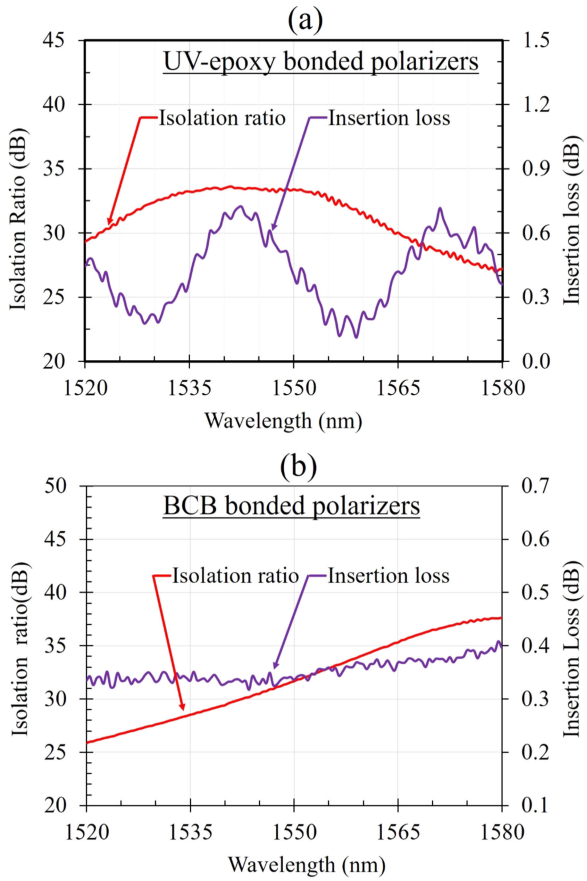

Fig. 6. Performance characteristics of bias-magnet-free bulk isolators (5 mm × 5 mm × 0.55 mm) with (a) UV bonded (a) and (b) BCB bonded Polarcor UltraThin polarizers.

the total input power. Optical loss and isolation performances were measured both at the slab waveguide level and for the ridge waveguides both with and without the polarizers. It was anticipated that the ridge waveguide would exhibit increased loss, relative to the slab, due to sidewall roughness and end facet quality. Samples that went through the BCB bonding process and FIB milling process reached or exceeded the 185°C Curie temperature for the MO material. For these samples, built-in poling of the bias-magnet-free MO material was reasserted by temporary application of a ∼4000 Oe magnetic field.

III. Performance Characteristics

A. BMF Bulk Isolator: UV Epoxy vs BCB-Bonded Polarizers

Polarcor ultraThin glass polarizers of size 2 mm × 1 mm × 30 μm were bonded onto the MO film facets via UV epoxy or BCB adhesive as depicted in Fig. 1. These bulk assemblies showed high isolation ratios and low insertion losses. In the UV epoxy bonded polarizer case (Fig. 6(a)), the isolation ratio was measured to be >30 dB in the range between 1522 to 1565 nm, and insertion losses were measured to be below 0.7 dB for the whole range. Fig. 6(b) shows the case for BCB bonded polarizers where the measured isolation was >25 dB, with a maximum of 38 dB at 1580 nm, and measured insertion loss was

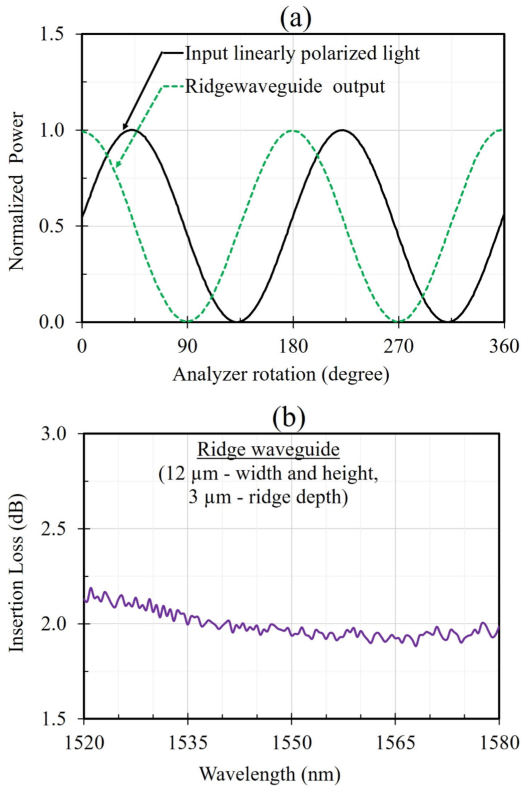

Fig. 7. Performance characteristics of FIB-fabricated ridge waveguide Faraday rotator (without Polarcor polarizers): (a) Faraday rotation and (b) insertion loss.

below 0.5 dB over the entire measurement spectrum. UV epoxy bonding was not considered a foundry compatible process nor as strong as BCB. Hence, BCB-bonded polarizer samples were used for subsequent device fabrication development. Sixty-μm-thin devices with BCB-bonded polarizers yielded isolation ratios ranging from 25 dB to 30 dB between 1525 nm to 1580 nm, with measured insertion losses varying between 0.6 dB and 1 dB in that wavelength range.

B. BMF Waveguide Faraday Rotators

Faraday rotation and insertion loss measurements were conducted on 12 μm thin ridge waveguides having 3 μm to 8 μm ridge-step depths. Waveguide operation was verified, with finite optical leakage and scattering losses due to top surface roughness. Fig. 7 shows the performance of a 3 μm ridge-step waveguide and 15 μm inter-waveguide gaps. The linearly polarized input light was rotated by about 46° by the Faraday ridge waveguide, yielding an effective double-pass polarization extinction ratio greater than 25 dB. The measured insertion loss was less than 2 dB. It is anticipated that insertion loss $<$1 dB may be achieved through optimization of the lap polish and ion beam etching processes.

C. BMF Waveguide Isolator

Optical test results for 12 μm thin slab waveguide and 12 μm thin ridge waveguide isolator structures are shown in Fig. 8.

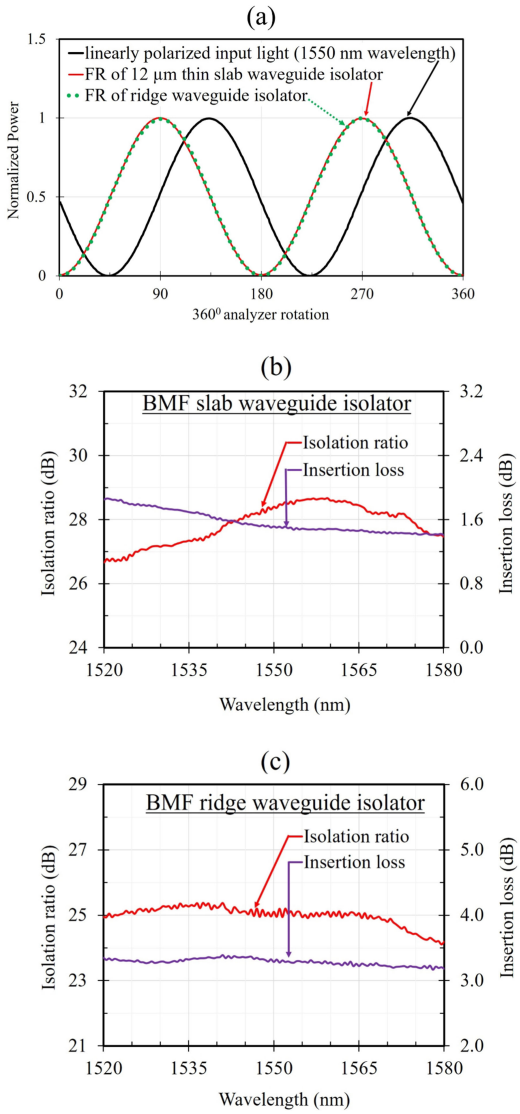

Fig. 8. Performance characteristics of bias-magnet-free isolators: (a) Faraday rotation of 12 μm thin slab and ridge waveguide structures, (b) insertion loss and isolation ratio of slab waveguide isolator, and (c) insertion loss and isolation ratio of ridge waveguide isolator (12 μm width and 3.6 μm ridge step).

Both the slab and ridge waveguides preserved 45° polarization rotations as in the bulk film, despite the sample having gone through mechanical polishing and FIB processing (Fig. 8(a)). Comparing the results of Fig. 8(b) and Fig. 8(c), the slab waveguide device can be seen to have an overall higher isolation and lower loss relative to the ridge waveguide. These features may be attributed to sidewall and end facet related scatter losses in the ridge guide and to finite ridge waveguide mode birefringence. Effects of fiber mode mismatch can also be expected to increase in the ridge guide, relative to the slab guide, due to the increased confinement. For comparison, free space bulk isolators feature a minimum isolation of 30 dB over the C-band, and maximum insertion loss of 0.5 dB. It is notable that the approximately 25 dB isolation in the single stage ridge guide is already approaching that for bulk isolators, despite the asymmetry in the waveguide height (12 μm) and width (15 μm). Improved fabrication

processes and mode matching are expected to further improve ridge guide isolation to 30 dB and optical insertion loss to less than 1 dB.

The effect of linear and modal birefringence on isolation performance was operative in the fabricated ridge waveguides reported here. Optical isolation in the as-purchased BMF plates of the same material (480 μm thick, 1 cm^2 plates) was >30 dB, as shown in Fig. 6(b) and in [30]. Fig. 8 showed that the slab isolator produced just under 30 dB isolation, whereas the ridge waveguide isolation was measured to be ~25 dB. Some of this reduction in isolation performance may be attributed to finite waveguide birefringence, which can increase as the level of confinement and mode asymmetry increases. However, beam propagation method simulation of the linear birefringence between transverse-electric (TE) versus transverse-magnetic (TM) fundamental modes for the ridge waveguide yielded a mode index difference of only 0.000023. This miniscule birefringence, due to the relatively large waveguide cross-section compared to the wavelength, indicated higher-order modes and sidewall scattering was primarily responsible for the lower 25 dB isolation ratio in the ridge waveguide, relative to the slab guide [30]. Judicious optimization of both the ridge design and the ridge fabrication process are expected to virtually eliminate these effects to produce isolation approaching that for bulk.

D. BMF Faraday Rotator Mirrors

Fabricated Faraday mirrors may be used for single-sided optical isolators, with properly engineered polarizer axes at 45° relative to each other on the front facet. Tests on 45° Faraday mirrors, as shown schematically in Fig. 3, were conducted.

The polarization rotation of the light before mirror coating and in one single pass was 22.5° as expected from 243 μm length of MO film along propagation direction (Fig. 9(a)). Polarization rotation due to double pass (incidence + reflection) from the same sample with the silver mirror backside coating was ~45° with ~30 dB extinction coefficient. The characterization was conducted for a ~5° angle of incidence to create room for the analyzer/photodetector measurements without blocking the incident beam. The extinction coefficient is expected to be higher for normal incidence as linear polarization is best maintained at normal incidence. The insertion loss for reflection-mode Faraday rotator devices was below 0.2 dB, as shown in the scanned spectral range plot in Fig. 9(b). Insertion loss differences with single-path rotators in the previous section stem from slab waveguide character and the presence of polarizers in the latter. The reflectors are bulk wafers (not slab waveguides, and no polarizers). The waveguide structure and processing plus the polarizers contribute to the additional loss.The indices of refraction of the polarizer material, BCB and the MO films are 1.51, 1.54 and 2.32 respectively. The MO material is anti-reflection (AR) coated to match the index of the BCB bonding layer to minimize the reflection losses at the interface.

E. Integration onto a PIC Platform

The ridge waveguide isolators demonstrated here may be integrated with other optoelectronic elements on a common silicon photonic platform using the same etched pocket, drop-in alignment and die bond attachment technique used to integrate III-V sources and detectors. The MO waveguides in the current work are designed to match standard SMF fibers and, as such, are expected to couple efficiently to standard silicon photonic fiber edge coupler elements. Another aspect of integration is that, with many silicon photonic platforms, the dropped in die must be single ended, with all optical ports being on a single facet. The Faraday rotator mirror test results reported in this paper have proven that a single ended integrated optic isolator may be realized simply by implementing end facet or on-chip mirrors to provide a return path for the light.

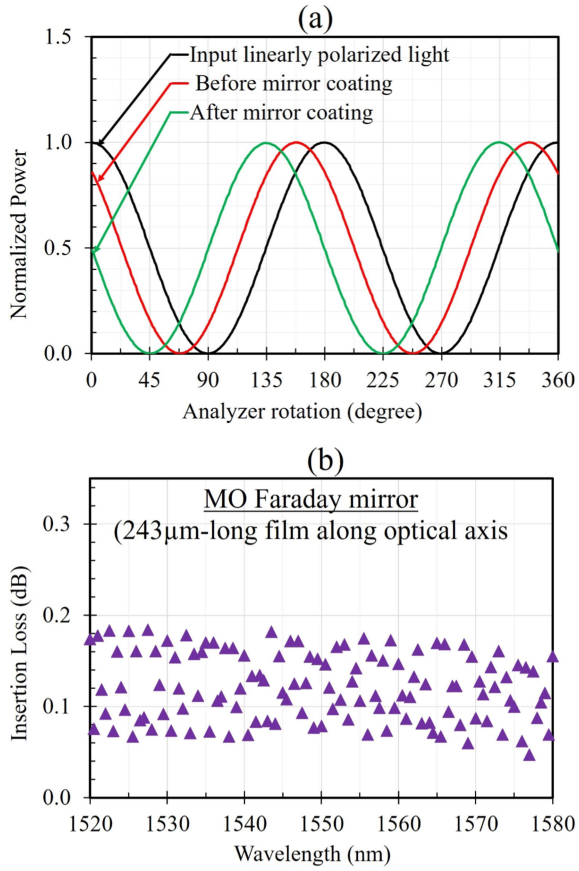

Fig. 9. Performance characteristics of 45° Faraday rotator mirror: (a) Faraday rotation of 243-μm-long MO material along optic axis. (b) Insertion loss of the film after mirror coating.

IV. Conclusion

Bias-magnet-free thin film waveguide isolators were demonstrated, with slab waveguide isolators exhibiting 29 dB isolation and total insertion loss of 1.5 dB. Ridge waveguide isolators exhibited 25 dB isolation and insertion loss just over 3 dB. These included fiber mode mismatch losses, scattering losses due to roughness, imperfection of the ridge waveguide structure and possible ion implantation related absorption from FIB milling. It is anticipated that improved fabrication and mode matching will produce ridge waveguide devices with isolation ratios over

30 dB and optical insertion losses below 1dB. The integrated polarizers make these devices compatible with any linearly polarized input simply by aligning the input polarizer to the desired input polarization state.

ACKNOWLEDGMENT

The views expressed are those of the authors and do not reflect the official policy or position of the Department of Defense or the U.S. Government. The U.S. Government is authorized to reproduce and distribute reprints for Governmental purposes notwithstanding any copyright notation thereon. Part of the work was conducted using Michigan Tech. University's microfabrication facility (MFF) and applied chemical and morphological analysis laboratory (ACMAL). The authors would like to thank S. Subramanian of II–VI, Inc. for valuable discussions.

REFERENCES

[1] L. Bi, J. Hu, G. F. Dionne, L. Kimerling, and C. A. Ross, "Monolithic integration of chalcogenide glass/iron garnet waveguides and resonators for on-chip nonreciprocal photonic devices," *Proc. SPIE 7941, Integrated Optics: Devices, Materials, Tech. XV*, Jan. 2011, Art. no. 794105, doi: 10.1117/12.875184.

[2] A. D. Block, P. Dulal, B. J. H. Stadler, and N. C. A. Seaton, "Growth parameters of fully crystallized YIG, Bi:YIG, and Ce:YIG films with high faraday rotations," *IEEE Photon. J.*, vol. 6, no. 1, Feb. 2014, Art. no. 0600308.

[3] M. C. Onbasli *et al.*, "Optical and magneto-optical behavior of cerium yttrium iron garnet thin films at wavelengths of 200–1770 nm," *Sci. Rep.*, vol. 6, 2016, Art. no. 23640.

[4] P. Dulal *et al.*, "Optimized magneto-optical isolator designs inspired by Seedlayer-Free terbium iron garnets with opposite chirality," *ACS Photon.*, vol. 3, no. 10, pp. 1818–1825, 2016.

[5] X. Y. Sun *et al.*, "Single-step deposition of Cerium-substituted yttrium iron garnet for monolithic on-chip optical isolation," *ACS Photon.*, vol. 2, no. 7, pp. 856–863, 2015.

[6] T. Mizumoto, R. Baets, and J. E. Bowers, "Optical nonreciprocal devices for silicon photonics using wafer-bonded magneto-optical garnet materials," *MRS Bull.*, vol. 43, no. 6, pp. 419–424, 2018.

[7] P. Pintus, D. Huang, P. A. Morton, Y. Shoji, T. Mizumoto, and J. E. Bowers, "Broadband TE optical isolators and circulators in silicon photonics through Ce:YIG bonding," *J. Lightw. Technol.*, vol. 37, no. 5, pp. 1463–1473, Mar. 2019.

[8] Y. Shoji and T. Mizumoto, "Silicon waveguide optical isolator with directly bonded Magneto-Optical garnet," *Appl. Sci.*, vol. 9, no. 3, pp. 1–8, Feb. 2019.

[9] B. J. H. Stadler and T. Mizumoto, "Integrated Magneto-Optical materials and isolators: A review," *IEEE Photon. J.*, vol. 6, no. 1, Feb. 2014, Art. no. 0600215.

[10] Q. Du *et al.*, "Monolithic On-chip Magneto-optical isolator with 3 dB insertion loss and 40 dB isolation ratio," *ACS Photon.*, vol. 5, no. 12, pp. 5010–5016, 2018.

[11] R. Yamaguchi, Y. Shoji, and T. Mizumoto, "Low-loss waveguide optical isolator with tapered mode converter and magneto-optical phase shifter for TE mode input," *Opt. Express*, vol. 26, no. 16, pp. 21271–21278, 2018.

[12] Y. Shoji, A. Fujie, and T. Mizumoto, "Silicon waveguide optical isolator operating for TE mode input light," *IEEE J. Sel. Topics Quantum Electron.*, vol. 22, no. 6, pp. 264–270, Nov./Dec. 2016.

[13] S. Ghosh, S. Keyvaninia, Y. Shirato, T. Mizumoto, G. Roelkens, and R. Baets, "Optical isolator for TE polarized light realized by adhesive bonding of Ce:YIG on Silicon-on-Insulator waveguide circuits," *IEEE Photon. J.*, vol. 5, no. 3, Jun. 2013, Art. no. 6601108.

[14] Y. Zhang *et al.*, "Monolithic integration of broadband optical isolators for polarization-diverse silicon photonics," *Optica*, vol. 6, no. 4, pp. 473–478, 2019.

[15] D. Huang, P. Pintus, and J. E. Bowers, "Towards heterogeneous integration of optical isolators and circulators with lasers on silicon [Invited]," *Opt. Mater. Express*, vol. 8, no. 9, pp. 2471–2483, 2018.

[16] J. Fujita, M. Levy, R. M. Osgood Jr, L. Wilkens, and H. Dötsch, "Waveguide optical isolator based on Mach-Zehnder interferometer," *Appl. Phys. Lett.*, vol. 76, 2000, Art. no. 2158.

[17] D. Huang, P. Pintus, Y. Shoji, P. Morton, T. Mizumoto, and J. E. Bowers, "Integrated broadband Ce:YIG/Si Mach–Zehnder optical isolators with over 100 nm tuning range," *Opt. Lett.*, vol. 42, no. 23, pp. 4901–4904, 2017.

[18] Y. Shoji and T. Mizumoto, "Magneto-optical non-reciprocal devices in silicon photonics," *Sci. Technol. Adv. Mater.*, vol. 15, no. 1, 2014, Art. no. 014602.

[19] Y. Shoji, K. Miura, and T. Mizumoto, "Optical nonreciprocal devices based on magneto-optical phase shift in silicon photonics," *J. Opt.*, vol. 18, no. 1, 2015, Art. no. 013001.

[20] D. Huang, P. Pintus, C. Zhang, Y. Shoji, T. Mizumoto, and J. E. Bowers, "Electrically driven and thermally tunable integrated optical isolators for silicon photonics," *IEEE J. Sel. Topics Quantum Electron.*, vol. 22, no. 6, pp. 271–278, Nov./Dec. 2016.

[21] D. Karki, R. El-Ganainy, and M. Levy, "Toward high-performing topological edge-state optical isolators," *Phys. Rev. Appl.*, vol. 11, no. 3, 2019, Art. no. 034045.

[22] "IR free-space isolators," 2019. [Online]. Available: https://www.thorlabs.com/newgrouppage9.cfm?objectgroup_id=4916, Accessed: Nov. 1, 2019.

[23] C. Zhang, P. Dulal, B. J. H. Stadler, and D. C. Hutchings, "Monolithically-integrated TE-mode 1D Silicon-on-insulator isolators using seedlayer-free Garnet," *Sci. Rep.*, vol. 7, no. 1, 2017, Art. no. 5820.

[24] K. Srinivasan and B. J. H. Stadler, "Magneto-optical materials and designs for integrated TE- and TM-mode planar waveguide isolators: A review," *Opt. Mater. Express*, vol. 8, no. 11, pp. 3307–3318, 2018.

[25] A. H. Atabaki *et al.*, "Integrating photonics with silicon nanoelectronics for the next generation of systems on a chip," *Nature*, vol. 556, no. 7701, pp. 349–354, 2018.

[26] M. Levy, R. M. Osgood, H. Hegde, F. J. Cadieu, R. Wolfe, and V. J. Fratello, "Integrated optical isolators with sputter-deposited thin-film magnets," *IEEE Photon. Technol. Lett.*, vol. 8, no. 7, pp. 903–905, Jul. 1996.

[27] D. Huang *et al.*, "Dynamically reconfigurable integrated optical circulators," *Optica*, vol. 4, no. 1, pp. 23–30, 2017.

[28] C. D. Brandle Jr, V. J. Fratello, and S. J. Licht, "Article comprising a magneto-optic material having low magnetic moment,", U.S. Patent 5 801 875, Sep. 1998.

[29] R. R. Abbott, V. J. Fratello, S. J. Licht, and I. Mnushkina, "Article comprising a Faraday rotator that does not require a bias magnet," U.S. Patent 6 770 223 B1, Aug. 2004.

[30] D. Karki, V. Stenger, A. Pollick, and M. Levy, "Thin-film magnetless Faraday rotators for compact heterogeneous integrated optical isolators," *J. Appl. Phys.*, vol. 121, no. 23, 2017, Art. no. 233101.

Dolendra Karki received the Ph.D. degree in physics from Michigan Technological University (MTU), Houghton, MI, USA, in 2018. He is a Postdoctoral Research Fellow with the Department of Physics, MTU. His current research is focused on experimentation on magnetic-garnet and silicon material-based nonreciprocal photonics devices.

Vincent Stenger received the Ph.D. degree in electrical engineering from the University of Cincinnati, Cincinnati, OH, USA, in 2003. He is the Principal Research Engineer with SRICO, Inc, Columbus, OH, where he is a key developer of innovative materials processing, device fabrication techniques, and device packaging. His professional activities are currently focused on heterogeneous and hybrid integration of thin film modulators and isolators.

Andrea Pollick received the B.S. degree in biomedical engineering from Marquette University, Milwaukee, WI, USA, in 2000. She has been with SRICO, Inc. since 2000 where she has tested, fabricated, and assembled optoelectronic components for SRICO's photonic system products. She is a Member of the Optical Society of America.

Miguel Levy received the Ph.D. degree in physics from the City University of New York, New York, NY, USA, in 1988. He is a Professor of Physics and Materials Science with the Michigan Technological University, Houghton, MI, USA. His research centers in photonics, with an emphasis on magneto-photonics and nonreciprocal phenomena. He is a Fellow of the Optical Society of America.